# Time-Integrated Light Images of OMEGA Implosions

## Introduction

Beginning in the spring of 2001, a series of remarkable photographs were taken that clearly show spherical target implosions as they might appear to the naked eye. Not surprisingly, the spherical target itself is not visible. The dominant feature in the photographs is the reflection of the laser beams hitting the target. These reflections appear as bright spots of light, organized in a very symmetric pattern.

These first experimental photographs, taken with aesthetics in mind more than quantitative measurement, were part of a series of visually appealing photographs of the inside of the target chamber. They represent a time-integrated picture of the target shot, from beginning to end (Fig. 89.1).

Upon closer scrutiny these photographs are found to contain useful and interesting information about the interaction of the laser beams with the plasma. The location and brightness of the spots as well as the number that are visible raised some questions, and the explanations were not intuitively obvious.

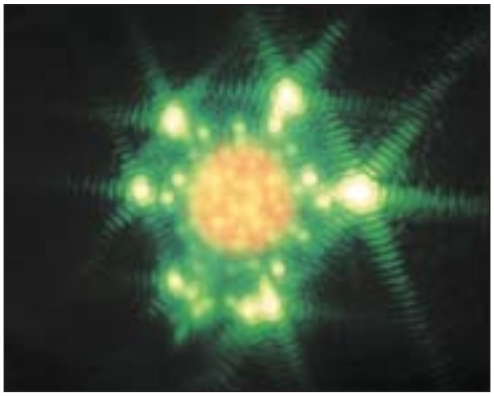

E11509

Figure 89.1
A time-integrated photograph showing a spherical target implosion. Beam reflections dominate the image and provide useful information about laser–plasma interactions. The concentric rings and spokes around each spot are camera artifacts. Note that almost 60 spots are visible, despite this being a picture of only one side of the target.

In light of this, an effort was made to make the photographs more quantitative. A UV transmission filter was added to the camera, and the film was switched from color to monochromatic, which allows a quantitative evaluation of the images. The filter passed 351-nm light, corresponding to the incident laser wavelength (Fig. 89.2).

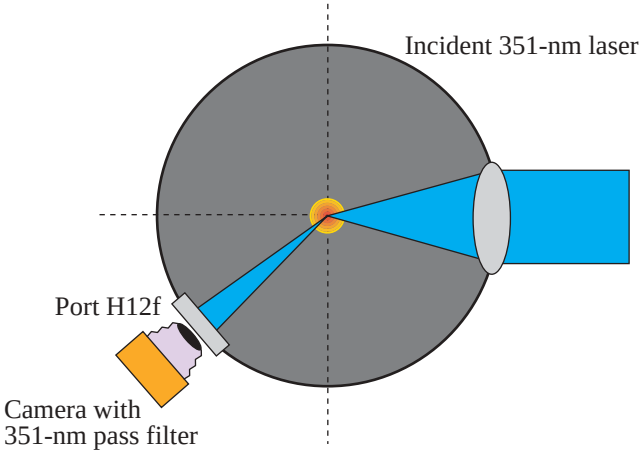


E11510

Figure 89.2
A rough layout of the experiment. Laser beams enter the target chamber and strike the spherical target. Reflections from the beams are seen and recorded by the camera in port H12f.

At the same time, in an effort to simulate the images, a program was written that performs ray tracing and absorption on the simulated laser beams. This program is designed to show whether the usual physical assumptions about laser–plasma interactions can explain the main features of the photographs. The simulation also adds time resolution to the images, explaining the photographs in a new light.

## Experiment

The first photographs (Fig. 89.1) were taken on color film by a camera mounted on a port outside of the target chamber. This port is slightly off center from a symmetry axis and contributes to a small asymmetry in the photographs. The

camera is operated in an unconventional way by adding a number of magnifying objective lenses in series. This makes it difficult to know precisely what the actual *f* number and focal length are, particularly since the objectives were not designed for 351-nm light.

Several qualitative features, however, are apparent immediately, the most important being that each spot is very distinct and corresponds to one particular laser beam. The outer spots appear to be larger and brighter than the inner spots, and the target itself is washed out. The origin of the soft circular glow in Fig. 89.1 cannot be easily identified, but it does not accurately portray the size of the target. When color film is used, the area appears red. This may be light scattered from the quarter-critical surface due to either Raman scattering or the two-plasmon-decay instability.

Perhaps the most-interesting feature is that all 60 beam spots are visible, which, considering that the photograph shows only one side of the target, was not expected. It means that the beams behind the target are visible as well as the beams incident on the front of the target. This is especially striking considering that the target turns opaque long before the laser pulse reaches its maximum.

The addition of the UV filter and monochromatic film changed the look of the photographs (Fig. 89.3). The spots are much smaller and well defined, and several features are now visible that had been obscured. Most notable is the streaking of the outer spots, indicating that, over the course of the shot, these spots move appreciatively from their original position in the radial direction. These outer spots also overexposed the film, showing that they contain much more energy than the inner spots, which are barely visible in places.

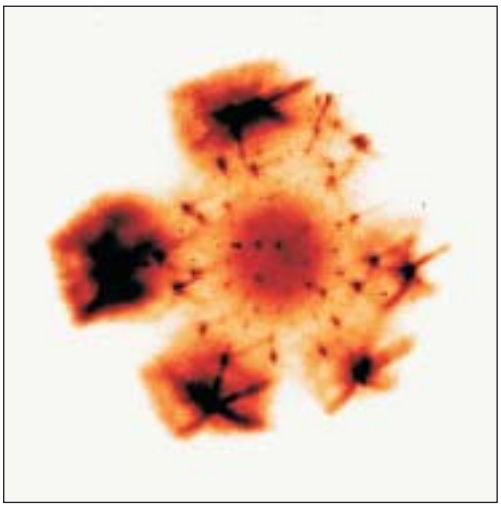

E11511

Figure 89.3
A UV photograph of the target implosion. This picture shows precise, small, clearly defined beam reflection spots. The outer spots suffer from overexposure and camera artifacts, masking some important details.

These monochromatic photographs were digitized for direct comparison to the output of the simulation.

**Theory and Simulation**

The index of refraction[1] of a plasma depends on the electron density, as shown in Eq. (1):

$$\mu = \sqrt{1 - n_e / n_c}\,, \tag{1}$$

where $\mu$ is the index of refraction, $n_e$ is the electron density, and $n_c$ is the critical density where the local plasma frequency equals the incident light frequency. A beam of light entering a region where $n_e > n_c$ will be reflected and/or absorbed at the critical-density surface. A ray of light passing through a plasma of density $n_e < n_c$ can be bent by refraction. Refraction depends on the direction of the ray and the direction and magnitude of the plasma density gradient.

This introduces the possibility that the laser beams striking the back of the target are refracted through the plasma into the camera lens. This is particularly likely since each laser spot is focused to be slightly bigger than the spherical target, with about 5% of the incident laser energy passing around the original target sphere. The beams striking the front of the target may be refracted and reflected as they approach the critical surface, again having their path bent into the camera lens. In this way, all 60 beams can become visible in the photograph.

The path of a ray through a medium of varying index of refraction is given by[2]

$$\frac{d}{ds}\left(\mu \frac{d\mathbf{x}}{ds}\right) = \nabla\mu \quad (\text{Snell's law}), \tag{2}$$

where $s$ is the path taken by the ray and $\mathbf{x}$ is the position vector along the path.

This equation can be rewritten in a form suitable for numerical simulation:

$$\mathbf{x}_{i+1} = \mathbf{x}_i + \frac{d\mathbf{x}_i}{ds} ds, \tag{3}$$

$$\mu_{i+1} \frac{d\mathbf{x}_{i+1}}{ds} = \mu_i \frac{d\mathbf{x}_i}{ds} + \nabla\mu(\mathbf{x}) ds. \tag{4}$$

Given the plasma density as a function of position, Eqs. (1), (3), and (4) are sufficient to trace the path of a ray through a plasma.

The simulation takes as input a *LILAC,* 1-D plasma density profile, which gives density as a function of radius. One density profile is given for each time step of 100 ps. The plasma is assumed to be stationary while the light passes through it. Once the density is read in, the index of refraction and its gradient are calculated as a function of radius.

Rays are then traced through this plasma by incrementing *ds* in small steps. Each laser beam is assumed to be focused in such a way that it is slightly wider than the target and composed of many parallel rays. Because the beams are slightly wider than the target, some rays strike the target center and are reflected straight back, some miss and go straight by, and the rest are scattered through the 180° between those two extremes.

Rather than tracing every possible path, the program iteratively throws away all the rays that do not land on the camera lens. After identification of the exact region of the laser that strikes the lens, this region is traced with many rays, yielding higher resolution.

The ray tracing can be done in two dimensions since any single ray remains in its plane of incidence. This plane is then rotated to trace out the full shape of the spot in the image. This process is then repeated for each laser beam. The position of the camera and the position of each beam are read in from a text file, making it easy to switch the parameters for different target shots.

The result of this ray tracing is translated into image space by taking into account the angle at which each ray strikes the camera lens. By rotating each beam and taking into account the geometry of the tank, the full 2-D photograph is reconstructed (Fig. 89.4).

This process is repeated in 100-ps steps until 1200 ps = 1.2 ns have passed. By this point the laser beam has switched off and no longer contributes to the image. The separate time-resolved images are saved and compiled into one time-integrated image to compare with the experimental data.

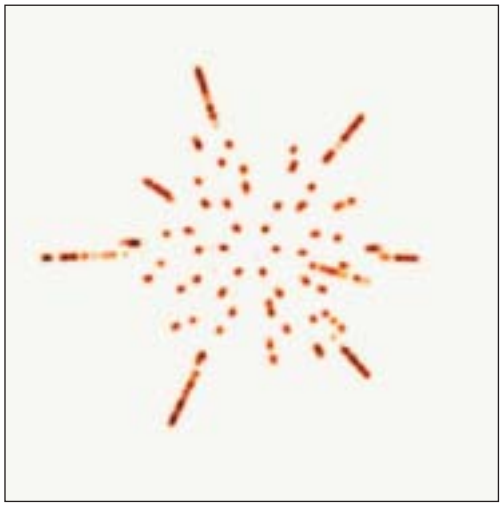

E11512

Figure 89.4
A simulated time-integrated image of an imploding target in the light of the 60 OMEGA beams driving it. This image shows the apparent locations of each beam reflection as seen from port H12f.

The simulations also allow for laser light absorption, via inverse bremsstrahlung in the plasmas:

$$\frac{dI}{ds} = -kI, \tag{5}$$

where the absorption coefficient[3]

$$k = \frac{16\pi Z^2 n_e n_i e^6 \ln\Lambda(\upsilon)}{3c\upsilon^2 \left(2\pi m_e k_b T\right)^{3/2} \left(1 - \upsilon_p^2/\upsilon^2\right)^{1/2}}. \tag{6}$$

The radial intensity distribution of the beam is approximated with a gaussian, yielding data about the beam power as it strikes the camera lens.

**Results**

The simulations are in good agreement with the experimental photograph (Fig. 89.5). The spots appear in the same symetrical pattern and show roughly the same relative levels of brightness.

The time resolution of the simulated images explains many of the features seen in the photograph. It is now apparent that most of the image is formed in the first 300 ps as a reflection from the solid sphere, with only a very thin plasma corona around it. As the plasma expands and fully forms, absorption takes over and the reflected intensity drops significantly. The outer beam spots seen in Figs. 89.1–89.4 are due to beams behind the target and their spill-over past the target. They suffer the least absorption as they are refracted into the camera. They are still clearly visible even at the end of the laser pulse, which explains the overexposure these spots produced on the film, as well as the outward radial displacement with time (Fig. 89.6).

**Conclusion and Discussion**

The simulation appears to explain most of the main features of the experimental photographs. The time resolution yields further information that was not available from the time-integrated photographs.

A careful comparison of the simulated images with the experimental photographs is limited by the setup of the camera. The camera has several objective lenses, making it difficult to know the exact path of the light through them. Port H12f of the target chamber is also not completely centered within the six beams surrounding it, leading to asymmetry in the photographs, which is duplicated in the simulation.

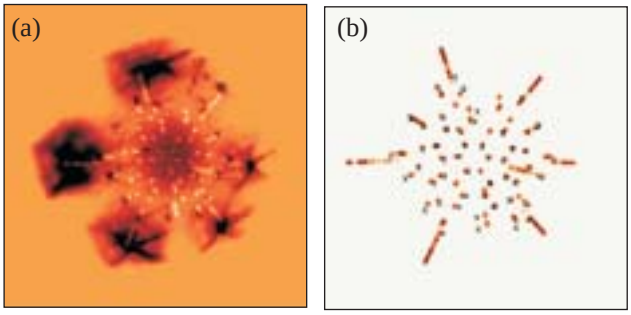


E11513

Figure 89.5
The remarkable agreement between simulated and actual photographs is apparent in the overlay of the simulations on the experimental image. Small disagreements in position and intensity are expected since the simulation is based on a 1-D plasma profile. In (b) small x's have been drawn on the simulated image corresponding to experimental spot position. Several predicted spots seem to be obscured on the experimental photograph. It is expected that with better camera equipment and filtering, these spots will be visible.

More importantly, however, an overall scaling problem was found with the camera. The exact scale of the experimental photographs is not completely certain. The photographs, taken on film, must be digitized in order to compare them with computer simulation.

In light of this, work has begun on a new camera designed to take quantitative digital photographs. This camera will be constructed of reflective optics, and the exact path of the light through it will be known. The simulation will be improved as well. When higher-quality images become available, it will be useful to add effects like plasma velocity and Doppler shifting to the code.

Further development of these ideas will likely address the potential of the new apparatus as a diagnostic for cryogenic target shots. The centering of the target, pointing of the beams, and early power-balance nonuniformities can all potentially be examined using this diagnostic. Further work will be devoted to determining the limits of the simulation and the experimental photographs.

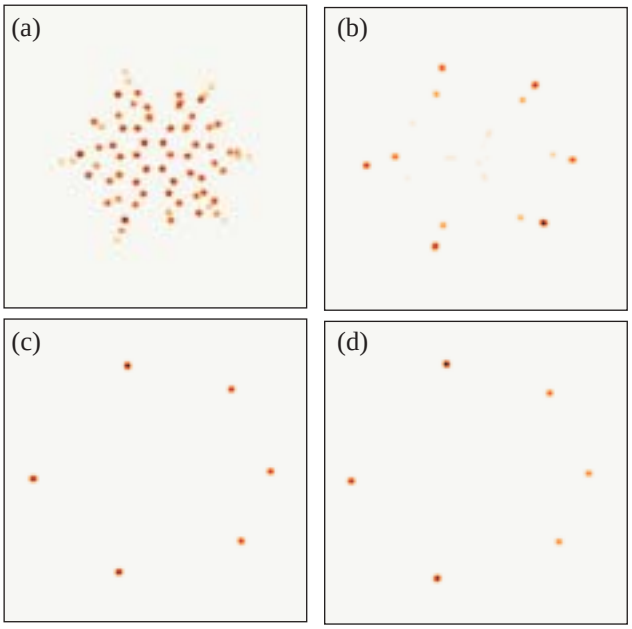


E11514

Figure 89.6
A series of simulated photographs showing the image seen by the camera at (a) 100 ps, (b) 400 ps, (c) 800 ps, and (d) 1100 ps. Reflection dominates until ~300 ps, when absorption in the plasma grows to almost 100%. From this point on, beams that refract from behind the target form most of the image.

## ACKNOWLEDGMENT

This work was supported by the U.S. Department of Energy Office of Inertial Confinement Fusion under Cooperative Agreement No. DE-FC03-92SF19460, the University of Rochester, and the New York State Energy Research and Development Authority. The support of DOE does not constitute an endorsement by DOE of the views expressed in this article.

## REFERENCES

1. F. F. Chen, *Introduction to Plasma Physics and Controlled Fusion*, 2nd ed., Vol. 1 (Plenum Press, New York, 1984).
2. M. Born and E. Wolf, in *Principles of Optics: Electromagnetic Theory of Propagation, Interference and Diffraction of Light*, 4th ed. (Pergamon Press, New York, 1970), pp. 121–123.
3. T. W. Johnston and J. M. Dawson, Phys. Fluids **16**, 722 (1973).